Synthetic Subsurface Pressure Derived from Bottom Pressure and Tide Gauge Observations

SABINE HARMS AND CLINTON D. WINANT

Center for Coastal Studies, Scripps Institution of Oceanography, University of California, San Diego, La Jolla, California

(Manuscript received 14 September 1993, in final form 31 March 1994)

ABSTRACT

Synthetic subsurface pressure (SSP) can be formed from tide gauge records and from bottom pressure measurements to provide a consistent and convenient basis for comparison of these two different types of observations. Common methods for this estimation are reviewed, and their accuracy is evaluated. Calculations show that subtidal SSP estimates from sea level (SSP_{SL}) and from bottom pressure observations (SSP_{BP}) at close sites agree only in a finite band of frequencies, corresponding to periods between 3.5 and 30 days. At the lower frequencies (periods longer than 30 days), sea level observations are subject to errors induced by the daily measure of staff height. At higher frequencies (periods between 1.5 and 3.5 days), the amplitude of fluctuations is too small to be resolved by a sea level gauge.

1. Introduction

Sea level measurements are of special interest in geophysical studies because few other records are as continuous or span such long timescales. Pressure gradients enter directly into the momentum equation, and once sea level has been related to pressure, gradients can be estimated, and their influence on forcing the circulation can be evaluated. Synthetic subsurface pressure (SSP) is defined as the pressure on a geoidal surface just beneath the sea surface.

Observations of subtidal SSP fluctuations or of adjusted sea level (ASL), the height equivalent to SSP, have been used to study the forcing of the coastal circulation. SSP or ASL observations are used by Allen and Smith (1981) and Lentz and Winant (1986) to describe the local response to wind forcing. Christensen et al. (1983), Chapman (1987), and Davis and Bogden (1989) use SSP fluctuations to separate remote from locally forced fluctuations in coastal currents. The seasonal variability in the SSP field has been described by Enfield and Allen (1980), and its relationship to the seasonal cycle of wind-driven currents has been examined by Strub et al. (1987). Hickey and Pola (1983) studied the role of alongshore SSP gradients in driving alongshore currents.

Sea level observations have been extensively used in the analysis of tides. Munk et al. (1970) analyzed tidal pressures and currents, as well as bottom pressures along the California coast, and established the amplitude and phase of the various components along the California coast.

Bottom pressure observations have been made with increasing frequency over the past decade, due in great part to the availability of stable pressure sensors. In contrast to measuring sea level, bottom pressure sensors measure absolute pressure directly, including the atmospheric component. They can be deployed in an anchoring system on the open shelf and benefit from the additional advantage of not being affected by local fluctuations such as can be introduced by harbor resonances, river runoff, and wind or wave setup. They are limited by possible vertical motions of the anchoring system.

Bottom pressure sensors measure the absolute pressure at the depth in which they are deployed including pressure changes due to density fluctuations in the water column above the sensor. This pressure must be subtracted from bottom pressure to obtain an estimate of SSP. Erdman (1983) described bottom pressure measurements on the California shelf and investigated the sensitivity of the measurement. Cross-shelf pressure gradients were estimated from pairs of observations and compared to related dynamical quantities. Brown et al. (1987) examined the relative roles of barotropic and density-related components of the pressure gradients obtained using bottom pressure observations and related these to the wind-driven coastal circulation regime off the coast of northern California.

To distinguish between SSP estimates from sea level and bottom pressure, the former are referred to as SSP_{SL} and the latter are referred to as SSP_{BP}. Pressure gradients are one of the forcing functions in the momentum equations, and the idea of combining the two

Corresponding author address: Dr. Clinton D. Winant, Center for Coastal Studies, Scripps Institution of Oceanography, University of California, San Diego, 9500 Gilman Drive, La Jolla, CA 92093-0209.

measures of SSP to estimate the large-scale pressure field is obviously attractive, but Agnew (1986) and Lentz (1993) have both reported difficulties arising during the analyses of SSP_{SL}. The work reported here compares SSP observations obtained from both sensor systems during the Northern California Coastal Circulation Study (NCCCS). First, the question how well SSP_{SL} reproduces SSP_{BP} observations at stations that are close is addressed. Second, discrepancies between SSP_{BP} and SSP_{SL} are examined to understand the differences as a function of frequency, for periods longer than 1.5 days.

The experiment and resulting observations are described in the next section. The method used to construct SSP_{BP} from bottom pressure and temperature measurements is described in section 3. Similarly, the calculation of SSP_{SL} from sea level and atmospheric pressure measurements is described in section 4. Summary and conclusions are presented in section 5.

2. Observations

a. *The experiment*

The NCCCS was designed to observe and quantify circulation patterns and the large-scale response of the circulation over the shelf and slope to wind and other forcing. The main program began in March 1988 and was completed in October 1989. The NCCCS region extends a distance of roughly 500 km from San Francisco to the Oregon border. Coastal circulation in the NCCCS region is affected by the varied topography and the wide range of meteorological conditions that occur there. The shelf is narrow compared to other shelves bordering the North American continent, with an average width of 20 km. Two major promontories, Cape Mendocino and Point Arena, interrupt the otherwise generally straight coast and mark changes in the orientation of the coast. The Mendocino escarpment lies perpendicular to the shore and rises over a distance of roughly 100 km from 2000 m north of the cape to a plateau of 500-m depth west of the cape (Fig. 1).

The design of the NCCCS was guided by the results obtained during the Coastal Ocean Dynamics Experiment (CODE) between 1981 and 1982. CODE was conducted in a small subregion of the NCCCS on the straight section of coast south of Point Arena. The CODE program provided detailed observations of currents, bottom pressures, temperatures, and winds. A major result of CODE was that water properties, currents, and pressures in this area are much more uniform in the alongshelf than cross-shelf or vertical directions (Brown et al. 1983; Winant et al. 1987). Those results suggested that a moderately dense sampling transect in the cross-shelf and vertical directions in each embayment of the NCCCS region would be sufficient to describe the local response to forcing.

The moored array design consisted of a total of 16 moorings containing current meters, temperature, and bottom pressure sensors, deployed on five transects

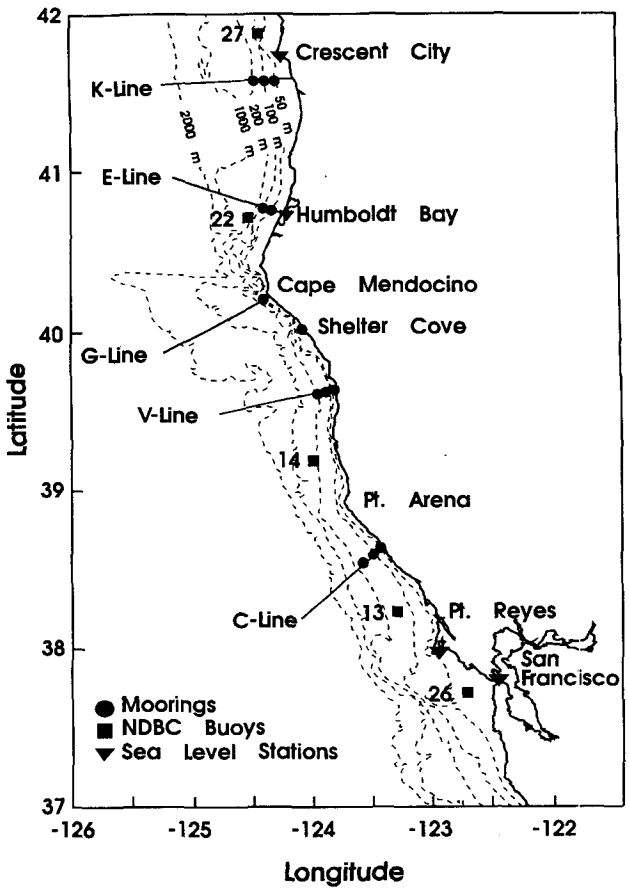

FIG. 1. NCCCS main moored instrument station locations and hydrographic transects, also showing meteorological and tide gauge stations within the NCCCS area.

crossing the continental shelf and upper slope. Each of the major embayments had a four-mooring transect: in the Eel River Basin at Klamath (K), in the Arena Basin at Cape Vizcaino (V), and in the Bodega Basin near Bodega (C for CODE). The C line is at the same location as the one used in CODE. In addition moored transects were sited to the north and south of Cape Mendocino at Eureka (E) and Punta Gorda (G) to resolve effects of the cape on the circulation pattern.

Moorings were deployed over the shelf at the 60-, 90-, and 130-m isobaths and over the slope at the 400-m isobath. Pressure sensors were located only over the shelf, so the 400-m mooring observations are not included in the analysis presented here. The locations and depths of the moored instruments are listed in Table 1. Throughout the paper the nomenclature for each instrument identifies location and depth, for example, V-60/10 refers to the instrument at 10-m depth on the 60-m mooring at the V line.

b. *Bottom pressure*

The bottom pressure array consisted of eight Paroscientific high-resolution quartz sensors deployed on

the 60- and 130-m moorings at the K, V, and C lines and on the 90-m moorings at the E and G lines. An additional bottom pressure sensor was deployed at Shelter Cove (SC) just south of Cape Mendocino at 10-m depth to serve as a coastal sensor in the absence of any sea level gauge between Point Reyes and Eel River (Table 1).

The pressure sensors used in this experiment were mounted inside anchors that consisted of three railroad wheels around a vertical hollow tube and are referred to by their upper operating limit (Table 1). The sensor consists of a mechanical coupling system that transmits outside pressure to a crystal, changing its resonant frequency. The output of the sensor is a square wave whose frequency varies from 36 to 40 kHz over the full-scale range of pressure. The number of cycles is counted over a 1-s period. The calibration equation is applied to convert the 1-s sum into pressure, and 1-min averages of pressure are recorded on cassette. During processing the pressure observations are averaged into hourly intervals.

Wearn and Larson (1982) showed that at a single test temperature, the pressures are accurate to within 70×10^{-6}–100×10^{-6} of the sensor's full-scale pressure: for the 31-, 138-, and 276-db sensors used in the NCCCS, an accuracy of 0.03, 0.14, and 0.28 mb can be achieved. The resolution of the Paroscientific pressure sensor, the smallest change that it can detect, is better than 4×10^{-8} of its full-scale pressure. This is equivalent to 0.12, 0.55, and 1.10 μb for the 31-, 138-, and 276-db sensors, respectively. Errors associated with voltage sensitivity and hysteresis are small; the size of error being less than 0.1 mb (Wearn and Larson 1982).

Drift and temperature sensitivity of the sensor appear to be the principal limitation in studying small pressure fluctuations. All pressure sensors used in the NCCCS have been operated several months prior to deployment to avoid initial drift of substantial amplitude due to irreversible aging and absorption. Following the application of a sustained high pressure, the pressure sensor output adjusts very rapidly to a new value and then drifts slowly in time. Wearn and Larson (1982) show that the drift of the pressure sensor, mainly due to elastic creep of the bellows under stress, is smooth, monotonic, reproducible, and reversible. Drift problems can be reduced substantially by skipping the first few days of data following deployment and detrending the rest of the data.

The error associated with the temperature sensitivity of the Paroscientific pressure sensors depends on both the temperature and the applied pressure. The errors introduced into the pressure records due to the sensor's temperature sensitivity are in general less than 1 mb per degree Celsius (the appendix). The pressure sensors were calibrated prior to and after the experiment at several temperatures ranging from 6° to 14°C, the smallest and largest possible temperatures that occur at the depth at which the sensors were deployed. To make corrections for the sensor's temperature sensitivity, the sensor's temperature was recorded during deployment, and a temperature dependent calibration equation was applied to the sensor's output.

TABLE 1. NCCCS moored instrument locations and equipment. The 400-m moorings are omitted. VMCM—vector measuring current meter; BP—bottom pressure sensor, the number in parentheses refers to the upper operational range of the sensor in decibars; T—temperature logger.

Location of transect	Station	Latitude (N)	Longitude (W)	Instrument depth (m)	Instrument type
Klamath	K-60	41°35.2′	124°16.9′	10	VMCM, T
				60	BP (138), T
	K-90	41°34.6′	124°21.6′	10, 45, 75	VMCM, T
	K-130	41°34.3′	124°26.1′	10, 75	VMCM, T
				130	BP (276), T
Eureka	E-60	40°47.4′	124°19.8′	10	VMCM, T
	E-90	40°48.7′	124°22.9′	10, 45, 75	VMCM, T
				90	BP (138), T
Shelter Cove	SC-10	40°01.0′	124°03.7′	10	BP (31), T
Punta Gorda	G-90	40°11.3′	124°21.7′	10, 45, 75	VMCM, T
				90	BP (138), T
Cape Vizcaino	V-60	39°38.8′	123°49.5′	10	VMCM, T
				60	BP (138), T
	V-90	39°38.6′	123°51.0′	10, 45, 75	VMCM, T
	V-130	39°38.1′	123°53.5′	10, 75	VMCM, T
				130	BP (276), T
Bodega	C-60	38°39.2′	123°25.3′	10	VMCM, T
				60	BP (138), T
	C-90	38°37.4′	123°27.5′	10, 45, 75	VMCM, T
	C-130	38°34.7′	123°31.3′	10	VMCM, T
				130	BP (276), T

During the NCCCS both long- and short-term noise was introduced into the bottom pressure records of several moorings due to movement of the anchor at the ocean floor. Some moorings were deployed on soft bottom, in which case the anchor settled slowly into the bottom. The resulting movement of the pressure sensor on the seafloor is smooth and occurs over several days, and the effects are difficult to remove from the data. Other anchors were dragged over on their side, presumingly due to fishing snag, and the vertical motion of the anchor is associated with an abrupt increase in the pressure signal.

Anchor shifts were removed from the bottom pressure time series before low-pass filtering the data. The problem in fixing anchor shifts is to find the right reference level of the shifted part of the time series. The time series before and after the anchor shift might have a different mean if a real trend exists over the whole time period. Since the bottom pressure signals are highly correlated across the shelf, the order 2–20-mb anchor shifts are detected by forming the cross-shelf difference between two bottom pressure time series measured along one transect (Fig. 2). A multiple linear regression model is used to predict the few data points over which the anchor shift occurred. To adjust the shifted part to the right reference level, the prediction is calculated up to a few hours after the anchor shift occurred. The shifted part of the time series is then adjusted to the predicted part such that the difference between the overlapping observed and predicted values is zero. The error introduced in the data by anchor shifts is believed to be smaller than 1 mb.

Because of the difficulty in determining an absolute reference level for the pressure observations the mean pressures are not meaningful, and they are removed from the bottom pressure signal. For the analysis of the subtidal shelf circulation the demeaned bottom pressure data are detided and low-pass filtered. Harmonic constituents calculated from the bottom pressure records are used to predict the tides at each mooring for the time period covered in the NCCCS. The predicted tides are then subtracted from the bottom pressure data. The detided time series are low-pass filtered using a PL64 filter, which removes fluctuations with periods shorter than 38 h (Limeburner 1985). Gaps in the bottom pressure time series are filled by multiple linear regression between records of neighboring stations.

c. *Sea level*

Sea level was measured at 13 National Ocean Survey (NOS) coastal sea level stations along the United States west coast. Four of these stations, the tide gauge stations at Crescent City, Humboldt Bay, Point Reyes, and San Francisco, are located within the NCCCS region (Fig. 1, Table 2).

All stations have been in continuous operation for at least 10 years. The tide gauges at Crescent City and San Francisco have been in operation for longer than 19 years. With the establishment of the tide gauge stations, a system of benchmarks is installed to which the observed tides may be referred. Published benchmark sheets available from NOS document the relative positions of the tidal datum planes and provide a relationship to a common geodetic datum.

The tide gauges, described by Lentz (1993) and others, are automatic float gauges, installed within stilling

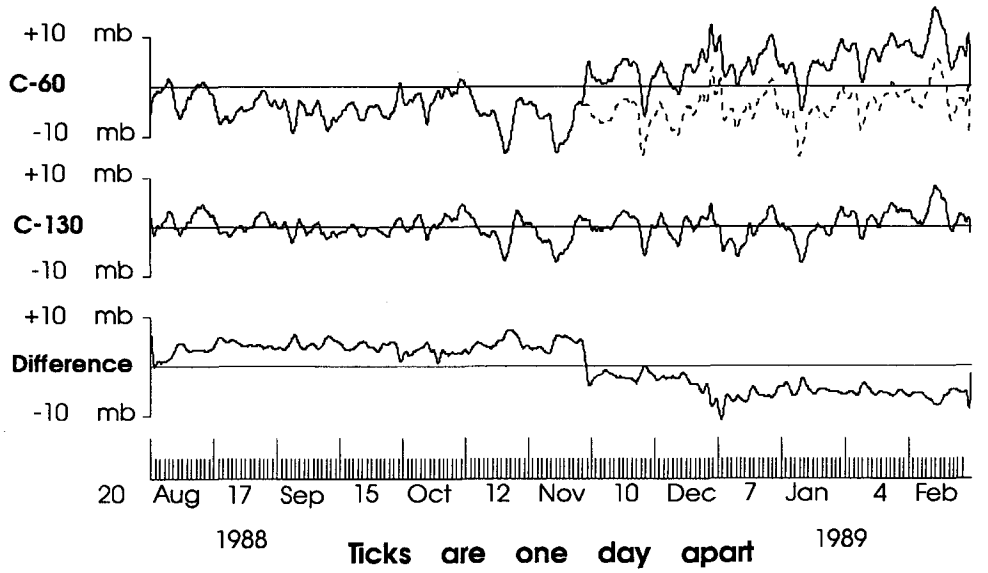

FIG. 2. Solid line: Time series of subtidal bottom pressure fluctuations at the C line (upper two panels) and their difference (lower panel). An anchor shift occurs at the C-60 bottom pressure sensor around 24 November 1988. Dashed line: Corrected time series of subtidal bottom pressure at the C-60 mooring. The correction has been applied to the raw bottom pressure data.

TABLE 2. NOS coastal sea level station locations and sources of barometric pressure observations used to adjust the sea level records.

Station name	Station ID	Latitude (N)	Longitude (W)	Barometric pressure source	Latitude (N)	Longitude (W)	Separation (km)
Crescent City	CR	41°44.7′	124°11.0′	NDBC 27 Pt. St. George	41°50.2′	124°23.8′	20.4
Humboldt Bay	HU	40°46.0′	124°13.0′	NDBC 22 Eel River	40°44.8′	124°30.1′	24.1
Point Reyes	PR	37°59.8′	122°58.5′	NDBC 13 Bodega	38°13.9′	123°18.1′	38.7
				NDBC 26 San Francisco	37°45.0′	122°41.5′	37.0
San Francisco	SF	37°48.4′	122°27.9′	NDBC 13 Bodega	38°13.9′	123°18.1′	87.1
				NDBC 26 San Francisco	37°45.0′	122°41.5′	20.1

wells that punch a paper tape every 6 min. The stilling well is a vertical tube with a small opening in the bottom, a few feet below the lowest probable tide, to admit the tide to a float operating the gauge while damping out higher frequency motions, such as induced by surface gravity waves. Each tide gauge station is equipped with a tide staff or equivalent float gauge to provide a temporary datum and reference scale for the automatic gauge record.

The quality of the observations of any tide gauge depends largely upon the observer in charge. The observer examines the tide gauge station daily to ascertain if it is operating properly. At the beginning of each calendar month the paper roll on the gauge is changed, and comparative time and staff readings are noted on the old and new rolls. After the record has been removed from the gauge the relation of its datum to the staff zero is determined by averaging the daily comparisons over the entire month. The preliminary scale setting and also any constant that may be necessary to refer to any datum other than staff zero is added to the monthly average of the daily comparisons. The algebraic sum of these quantities is used to correct for any changes in absolute height setting (C&GS 1965).

The tidal datum adopted for tide observations along the Pacific coast of the United States is the mean lower low water (MLLW), which is defined as the mean of the lower of the two low waters of each day over a considerable period of time. The tidal datum for the stations at Crescent City and San Francisco is established from 19-yr averages over the latest epoch from 1960 to 1978. The tidal datum for the remaining stations is computed over the available record length. The relationship between staff zero datum and MLLW is supplied by NOS. The recorded elevations are thus expressed relative to MLLW in units of feet where a positive difference indicates a datum plane at a higher elevation than MLLW.

At the float gauge the tidal heights are recorded with a resolution of 0.3 cm. The comparative readings are in general read with an accuracy of ±1.5 cm. The recorded elevations are averaged and subsampled at hourly intervals. Gaps in the records are filled by NOS using data from the backup gauges. If these are not available, small gaps, up to a few hours, are filled by linear interpolation. Larger gaps, up to 3 days, are filled by using data from neighboring stations. Gaps larger than 3 days are flagged by null values, indicating missing data.

For the analysis of subtidal sea level variability the time series are detided by removing the predicted tide calculated from 37 constituents obtained from a harmonic analysis of a year-long record. The detided time series are low-pass filtered using a PL33 filter, which removes fluctuations with periods shorter than 40 h. The detided, low-pass-filtered sea level observations are received from Magnell et al. (1989). A comparison study between PL33 and PL64 filters shows that both filters produce almost identical time series (Limeburner 1985).

3. Constructing SSP from bottom pressure and temperature

To compare the bottom pressure measurements to SSP measured at coastal sea level stations, bottom pressure is converted into SSP_{BP}; that is, the contribution of density fluctuations to pressure is subtracted from the bottom pressure measurements (Fig. 3). Assuming a hydrostatic pressure distribution in the vertical,

$$\frac{\partial P(z)}{\partial z} = -g\rho(z),$$

and integrating the hydrostatic equation over the water column,

$$P_{\text{bot}} = P_{\text{atm}} + \rho_0 g(\eta + H) + g\int_{-H}^{\eta} \rho' dz,$$

bottom pressure P_{bot} can be expressed as the sum of SSP $[=P_{\text{atm}} + \rho_0 g(\eta + H)]$ and baroclinic pressure. The baroclinic part of pressure involves the integral of the fluctuating part of density over the water column $\int_{-H}^{\eta} \rho' dz$, which is approximated here as $\int_{-H}^{0} \rho' dz$, since $\int_{0}^{\eta} \rho' dz$ is small, where $z = 0$ is the equilibrium sea level.

Time series of density are not available but density is a function of temperature that has been measured at all moored instruments. Based on previous observations in this region (Huyer 1984; Brown et al. 1987; Lentz 1993) density can be linearly related to temperature as

$$\Delta\rho = \Delta T \rho_0 \alpha, \quad \alpha = -3 \times 10^{-4}\ ^{\circ}\text{C}^{-1}.$$

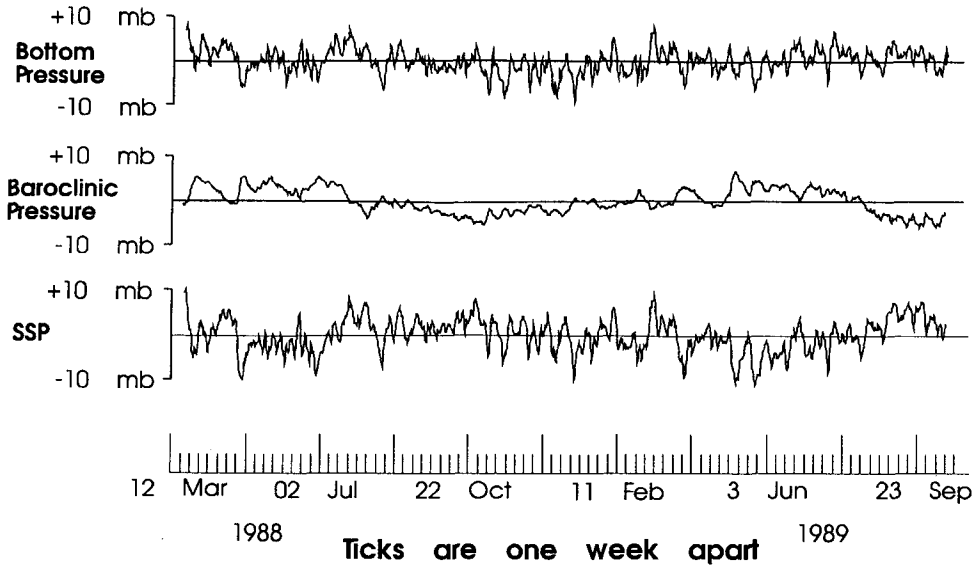

FIG. 3. Subtidal bottom pressure (upper panel), baroclinic pressure (middle panel), and synthetic subsurface pressure SSP_{BP} (lower panel) at the C-130 mooring.

Then the equivalent surface pressure is calculated as

$$SSP_{BP} = P_{bot} - \rho_0 g\alpha \sum_n (\Delta T_n)\Delta h_n,$$

where T_n represents temperature measurements at various depth intervals Δh_n.

Temperatures used to calculate the baroclinic pressure at each mooring are listed in Table 3. The correlation between temperature fluctuations measured along one transect at the same depth is 0.8 or larger. To improve the vertical resolution of the baroclinic pressure field, temperatures from the 90-m moorings are included in the calculation of baroclinic pressure at the 60- and 130-m moorings.

The contribution of baroclinic pressure, that is, of temperature effects, to bottom pressure leads to significant differences between SSP_{BP} and bottom pressure, especially at low frequencies (Fig. 4). The coherence between pressure fluctuations measured along different isobaths increases significantly for low-frequency motions with periods longer than 40 days after bottom pressure is converted into SSP_{BP}.

4. Constructing SSP from sea level and atmospheric pressure

To obtain the equivalent of total pressure, as measured by the bottom pressure sensors, an adjustment to include the barometric pressure must be made to the sea level records (Brown et al. 1985). The surface elevation η is expressed as an equivalent pressure due to the height of the water column. Barometric pressure of the atmosphere P_{atm} measured at or near the tide gauge station (Table 2) is then added, to yield SSP_{SL},

$$SSP_{SL} = P_{atm} + \rho_0 g\eta.$$

Due to gaps in the meteorological coverage, pressure records from two or more neighboring sources were concatenated for several of the sea level stations (Magnell et al. 1989). Time series of atmospheric pressure show that the spatial correlation of the pressure field is high over relatively large distances. Dobson (1980) shows that errors in the atmospheric pressure measurement are of order 0.1 mb. Lentz (1993) compares atmospheric pressure measurements at different locations in the Southern California Bight and finds that typical atmospheric pressure field variations are of order 0.01 mb km^{-1}. Localized studies (Dorman 1994, personal communication) suggest variations slightly larger in the CODE region and bay areas and variations smaller than 0.01 mb km^{-1} north of Cape Mendocino. Associated errors in SSP_{SL} due to station separation between barometric pressure and sea level measurements (Table 2) are of order 0.1 mb for stations north of Cape Mendocino and of order 1 mb for stations south of the cape.

The effect of the fluctuating surface temperature, T', on SSP_{SL} is examined by comparing SSP_{SL} calculated from a constant reference density ρ_0 to SSP_{SL} calculated from $\rho(T')$ as a function of surface temperature. The difference in density between ρ_0 and $\rho(T')$ is of order 0.1 kg m^{-3} and the influence of T' on SSP_{SL} is negligible.

a. The accuracy of tide gauge measurements

The accuracy of tide gauge measurements has been examined by several investigators (Lentz 1993; Agnew 1986; Shih and Porter 1981; Lennon 1967) who show that sea level measurements are subject to a variety of errors, some associated with inaccuracies in the mea-

TABLE 3. Temperatures and depth intervals used to calculate baroclinic pressure according to section 3.

Station name	T_n	Δh_n (m)
K-60	K-60/10	20
	K-90/45	30
	K-60/60	10
K-130	K-130/10	20
	K-90/75	70
	K-130/130	40
E-90	E-90/10	20
	E-90/45	30
	E-90/75	30
	E-90/90	10
SC-10	SC-10/10	10
G-90	G-90/10	20
	G-90/45	30
	G-90/75	30
	G-90/90	10
V-60	V-60/10	20
	V-90/45	30
	V-60/60	10
V-130	V-130/10	20
	V-90/75	70
	V-130/130	40
C-60	C-60/10	20
	C-90/45	30
	C-60/60	10
C-130	C-130/10	20
	C-90/75	70
	C-130/130	40

surement itself and others due to local peculiarities of the observational site.

To estimate the accuracy of tide gauge measurements within the NCCCS region, differences in subtidal SSP_{SL} between adjacent tide gauge stations are calculated. These differences, for example between the San Francisco and Point Reyes sea level stations, reveal yet another source of error (Fig. 5). Vertical lines indicate the dates when the data tapes were changed at either station. Abrupt changes in the pressure differences of the order of several centimeters appear as jumps right at the times when the records were changed.

Differences in the monthly mean values of sea level measured at Point Reyes and San Francisco are calculated over a 3-yr period, from January 1987 to December 1989, and are compared to differences in monthly means of SSP_{BP} measured at C-130 and V-130 (Fig. 6). Vertical, dashed lines indicate the time period during which the NCCCS took place. The differences of the monthly means of SSP_{SL} deviate generally ±3 mb from zero mean except in spring and summer of 1988, the beginning of the NCCCS program, when the values vary rapidly with maximum amplitudes of ±8 mb around the mean. In contrast, differences in monthly SSP_{BP} means fluctuate roughly

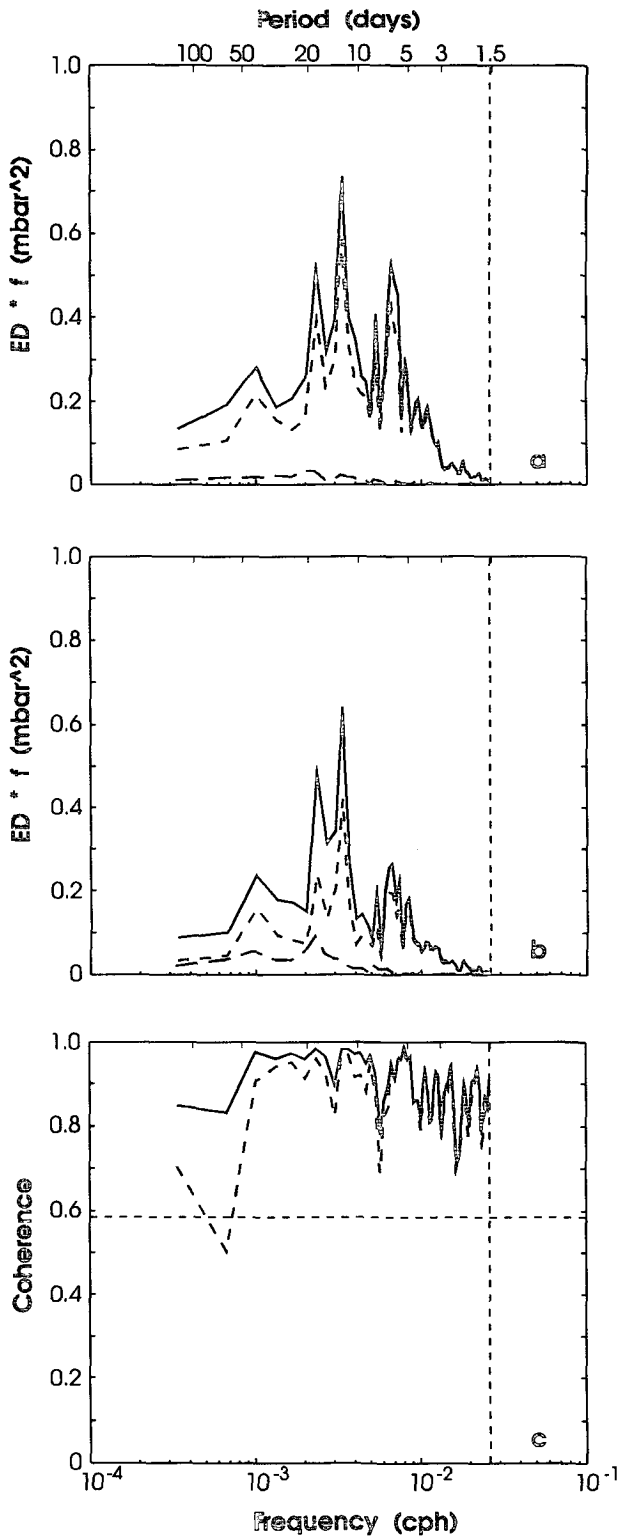

FIG. 4. Spectral densities of subtidal bottom pressure (dashed), baroclinic pressure (long dashed), and SSP_{BP} (solid) at (a) C-60 and (b) C-130. Spectra are normalized by multiplying the energy density by the frequency. (c) Coherence between subtidal SSP_{BP} at C-60 and C-130 (solid line). Superimposed is the coherence between bottom pressure at C-60 and C-130 (dashed line). The 95% confidence limit is 0.58, indicated by the horizontal dotted line.

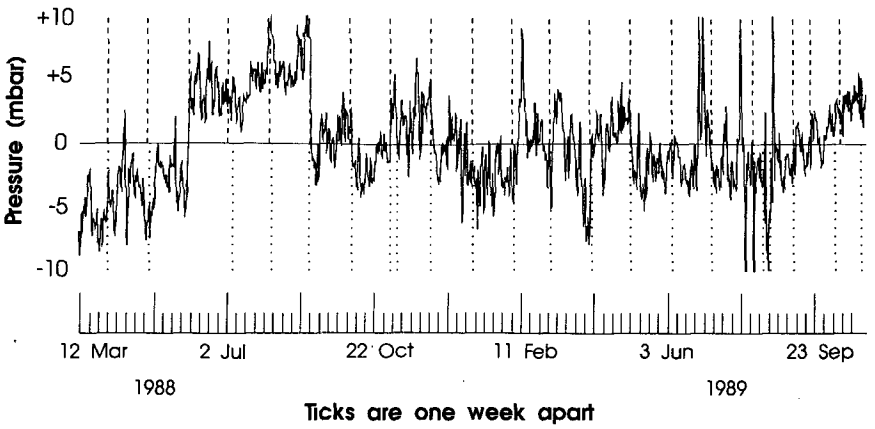

FIG. 5. Difference in SSP_{SL} between Point Reyes and San Francisco. Dashed lines (upper half) indicate the times when the San Francisco tide gauge records were changed; dotted lines (lower half) indicate the times when the Point Reyes data tapes were changed.

±1 mb from zero mean, their maximum amplitudes reaching only ±2 mb.

A comparison of SSP_{SL} and SSP_{BP} records identifies the order 10-mb jumps at the beginning of the NCCCS program as part of the San Francisco subtidal signal. The abrupt 10-mb increase in pressure in the San Francisco SSP_{SL} record at the beginning of June 1988, as well as the sudden decrease in pressure of similar magnitude three months later in September, appear exactly at times when the tide gauge was serviced.

This coincidence suggests the following: At the beginning of June the observer realized that the stilling well was clogged. When cleaning the float well it is necessary to remove the float from the well and, to avoid any tangling of the float wire when raising the float, to secure the wire by a clamp or loop around some convenient object to take up the slack. The float wire is rolled up onto the float drum, which is approximately 10 cm in circumference and has a threaded face to accommodate 30 turns of the float wire. It is likely that in the process of reinstalling the float, the observer missed one turn when rolling up the float wire onto the drum, resulting in a 10-cm increase in the tidal height measurement, which is equivalent to a 10-mb jump in pressure. Three months later, at the beginning of September, the observer realized his mistake and added one turn back onto the drum, explaining the corresponding decrease in pressure.

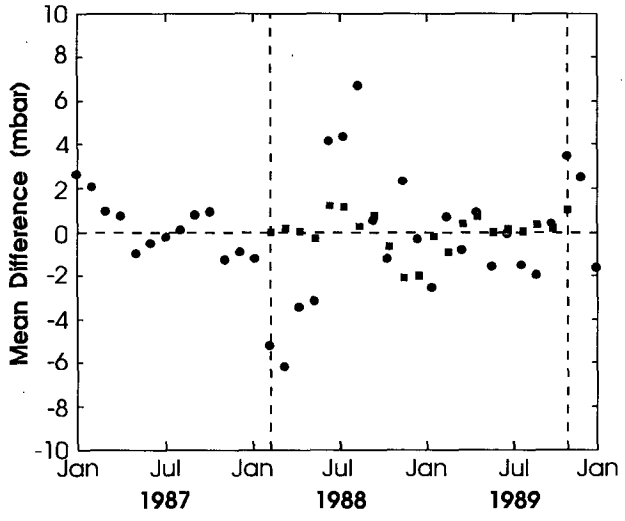

FIG. 6. Difference in monthly mean SSP_{SL} between San Francisco and Point Reyes (circles) and difference in monthly mean SSP_{BP} between C-130 and V-130 (squares). The NCCCS took place from March 1988 through October 1989, indicated by the vertical, dashed lines.

Smaller jumps of order 2–6 mb, in this example at the beginning of October, November, and December 1988 and at the beginning of April and May 1989 (Fig. 5) at times when the tide gauge stations were serviced, are not specific to one SSP_{SL} record but occur randomly in either of the two. Lentz (1993) suggested that these offsets are due to inaccuracies in estimating the monthly corrections to the reference level of sea level from the average of the independent daily readings (section 2c). Agnew (1986) observed similar large rapid changes in sea level in the Avila Beach tide gauge data in 1969 and showed that the source of the problem is the clogging of the stilling well.

These offsets in the time series with periods of the order of a month reduce the coherence between low-frequency SSP_{SL} fluctuations. The coherence between SSP_{SL} at Crescent City and Humboldt Bay and between SSP_{SL} at Point Reyes and San Francisco drops significantly for fluctuations with periods longer than 30 days (Fig. 7, dashed), whereas the coherence between SSP_{BP} fluctuations, calculated for a variety of stations separated in both along- and across-shelf directions, remains high at these low frequencies (Fig. 8).

To correct for the offsets, the differences between SSP_{SL} measured at the tide gauge station and bottom

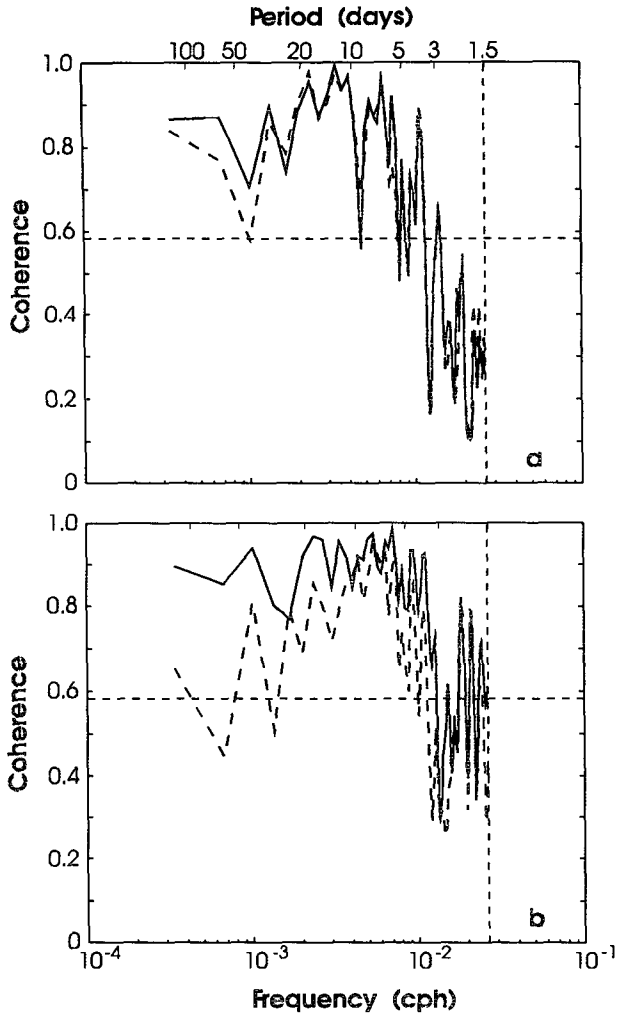

FIG. 7. Coherence between corrected subtidal SSP_{SL} at Crescent City and Humboldt Bay [(a), 108 km apart] and Point Reyes and San Francisco [(b), 50 km apart] (solid lines). Superimposed (dashed lines) are the coherences between original SSP_{SL} (as received from Magnell et al.). The 95% confidence limit is indicated by the dashed horizontal lines.

pressure from an adjacent moored instrument are formed. The shifted parts of the SSP_{SL} measurements are then adjusted according to the bottom pressure record such that at the jump the differences between both records are zero.

The most significant result is that the coherence between low-frequency SSP_{SL} fluctuations increases significantly once the offsets in the SSP_{SL} time series have been removed (Fig. 7, solid). In the following analysis, corrected SSP_{SL} is used only to represent the coastal SSP_{SL} field.

b. Noise level of tide gauge measurements

The coherence between corrected SSP_{SL} measurements at Crescent City and Humboldt Bay, as well as Point Reyes and San Francisco (Fig. 7), is statistically insignificant for subtidal fluctuations with periods shorter than 3.5 days, whereas the coherence between SSP_{BP} fluctuations in this band remains high (Fig. 8). It is suggested that the lack of coherence between SSP_{SL} fluctuations results from the limited resolution of the sea level measurements (section 2c).

Although the automatic float gauges record the tidal heights to ±0.3 cm, the accuracy of the measurements at these small scales is somewhat doubtful because the daily comparative readings, from which the reference level is calculated, are measured with an accuracy of only ±1.5 cm. Thus, the tidal heights are believed to be accurate to ±1.5 cm, which corresponds to fluctuations approximately equal to ±1.5 mb.

Sea level spectra show that in the 3.5- to 1.5-day band the sea level signal is very weak (Fig. 4). At these

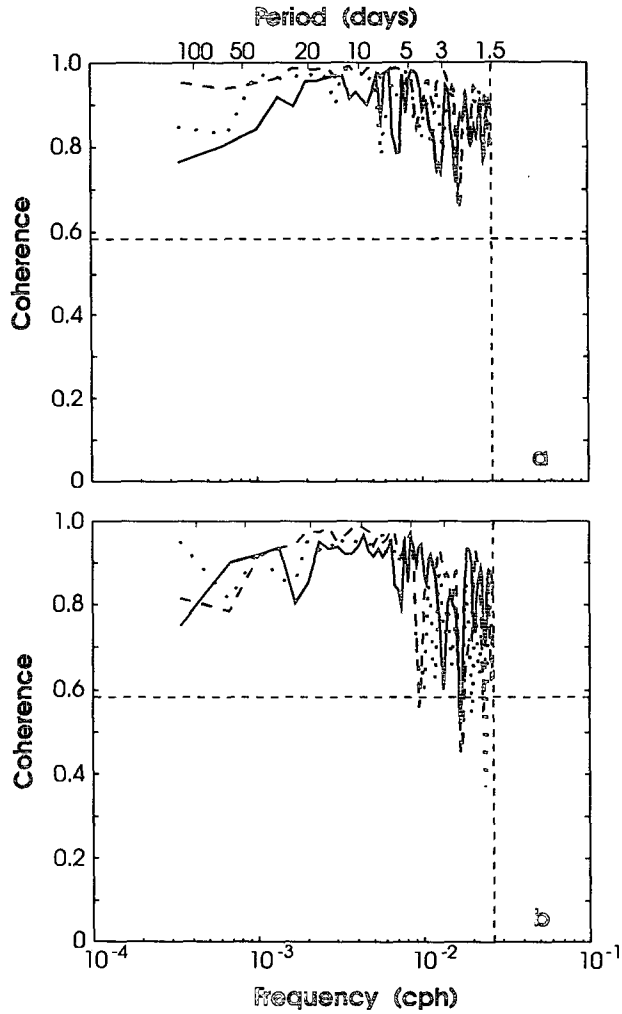

FIG. 8. Coherence between subtidal SSP_{BP} measured by bottom pressure sensors (a) along one transect [solid line: K-130 and K-60 (27 km apart); dashed line: V-130 and V-60 (6 km apart); dotted line: C-130 and C-60 (13 km apart)] and (b) separated in the alongshelf direction [solid line: K-130 and E-90 (86 km apart); dashed line: G-90 and V-130 (73 km apart); dotted line: V-130 and C-130 (123 km apart)].

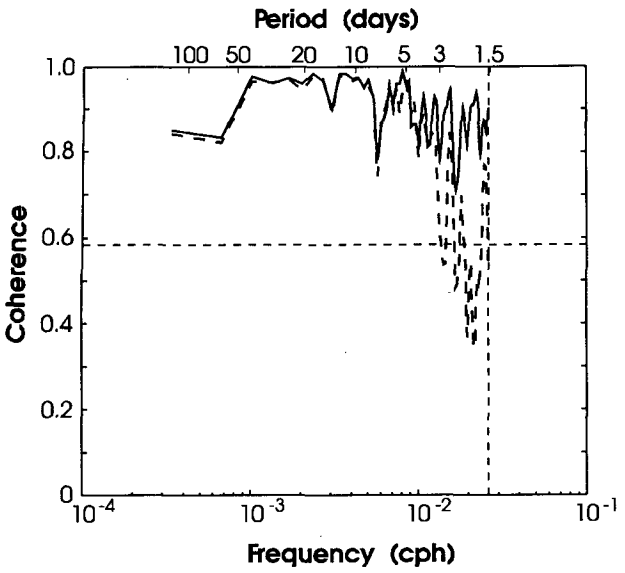

FIG. 9. Coherence between SSP_{BP} at C-60 plus additive white noise of ±1.5-mb amplitude and SSP_{BP} at C-130 (dashed line). Superimposed is the coherence between SSP_{BP} at C-60 and C-130 (solid line).

frequencies the noise level of the sea level measurement has the same order of magnitude as the energy level of the true signal. The ratios of the energy densities of noise and true signal are large, reducing the sample coherence between both sea level measurements well below the true coherence (Fig. 7). In contrast, the coherence between SSP_{BP} measurements is significant for fluctuations in the 3.5- to 1.5-day band (Fig. 8). The bottom pressure sensors resolve sea level fluctuations with an accuracy of ±0.1 to ±0.3 mb, depending on their upper operating limit (section 2b). Thus, although the energy level is low at these high frequencies, it is still large compared to the noise level of the measurement. As a consequence the energy density ratios are small and the sample coherence is high.

The conclusion that the limited resolution of tide gauge measurements is in fact responsible for the drop-off in coherence below the level of significant coherence is confirmed by the results obtained from the following computational experiment. White noise with an amplitude of ±1.5 mb is added to the SSP_{BP} record measured at C-60. Then the coherence between this "noisy" C-60 record and SSP_{BP} measured at C-130 is calculated (Fig. 9). The coherence becomes statistically insignificant for subtidal fluctuations with periods shorter than 3.5 days. The frequency at which the coherence between both measurements becomes insignificant decreases as the amplitude of the added white noise increases.

5. Summary and discussion

Tide gauges and bottom pressure sensors are frequently used to estimate pressure in the ocean, although neither sensor strictly measures the pressure in the water near the surface. We want to combine bottom pressure and sea level into a single set of observations and we have chosen SSP as the means to do this.

We estimate baroclinic pressure and subtract it from bottom pressure to obtain SSP_{BP} (section 3). SSP_{SL} is formed by converting sea level η into an analog of absolute pressure $\rho g \eta$ and adding the barometric pressure of the atmosphere (section 4). Comparing subtidal SSP_{BP} and SSP_{SL} fluctuations we find pronounced differences between both variables at frequencies lower than 30 days and higher than 3.5 days. We ascribe the lower-frequency discrepancies to observer problems and to errors in adjusting the sea level data to the reference level based on independent daily staff readings. Cross-comparisons with the SSP_{BP} time series allows us to remove these problems from the SSP_{SL} records. Differences at the high-frequency end of the SSP spectra are associated with the limited resolution of tide gauge measurements.

Amplitudes of bottom pressure and baroclinic pressure fluctuations in the NCCCS region are of similar magnitude (Fig. 3, Table 4) with standard deviations ranging roughly from 2 to 4 mb. Bottom pressure fluctuations are strongest at the coast and decrease in the offshore direction, baroclinic pressure fluctuations approximated as the vertical integral of temperature over the water column decrease toward the shore. While the subtidal bottom pressure variability on the northern California shelf is dominated by fluctuations with periods of order days to weeks, most of the baroclinic pressure variability is found on seasonal timescales, the pressure being at a maximum in the summer when the water column is strongly stratified and at a mini-

TABLE 4. Standard deviations of bottom pressure, baroclinic pressure, and their difference SSP_{BP} measured at moored instruments and of atmospheric pressure, SSP_{SL}, and corrected SSP_{SL} measured at coastal tide gauge stations. Units are in millibars.

Station ID	Bottom pressure (mb)	Baroclinic pressure (mb)	SSP_{BP} (mb)
K-60	4.0	1.5	4.2
K-130	3.1	2.6	3.6
E-90	3.1	1.7	3.6
SC-10	4.6	0.6	4.8
G-90	3.2	2.2	4.1
V-60	3.7	1.6	4.6
V-130	2.9	3.0	4.1
C-60	3.5	1.9	4.2
C-130	2.7	2.7	3.7

	Atmospheric pressure (mb)	SSP_{SL} (mb)	Corrected SSP_{SL} (mb)
CR	5.1	6.3	5.8
HU	4.8	5.6	5.0
PR	4.5	6.1	4.7
SF	4.3	5.4	4.3

mum in the winter when the water column becomes well mixed (Largier et al. 1993). The subtidal SSP_{BP} field is characterized by strong order 10-mb fluctuations on wind-driven (Largier et al. 1993) timescales, on which lower-frequency motions are superimposed.

Low-pass-filtered atmospheric pressure fluctuations have amplitudes comparable to those of the subtidal SSP_{SL} field with standard deviations of order 5 mb (Table 4). The major variations in atmospheric pressure occur on timescales of about a week, associated with the passage of the synoptic weather systems over the northeast Pacific. Most of the subtidal SSP_{SL} variability is found at timescales from a day to a few weeks and on seasonal timescales (Largier et al. 1993).

Subtidal SSP fluctuations in the NCCCS region are of order ± 10 mb and are significantly correlated over a wide range of frequencies (Fig. 10). Standard deviations, ranging from about 4 to 6 mb, are largest in the north and at the coast and decrease both toward the south and in the offshore direction (Table 4). Strong events with periods of the order of days to weeks dominate the SSP variability. These events are prominent over the entire NCCCS region, highly correlated, and have a clear phase propagation (Table 5). Lags correspond to phase speeds of approximately 5 m s^{-1} with which the SSP signal propagates poleward along the California coast. The annual variability in SSP seems to be associated with the heat content in the upper ocean (Largier et al. 1993). Annual and semiannual harmonics fitted to the SSP time series clearly identify the annual cycle of sea level variability, with generally higher sea level during late summer and early fall, that is, from August to October, and lower sea level during spring and early summer, that is, from April through July.

The high correlation between SSP_{BP} and SSP_{SL} at stations that are close (Table 5), correlation coefficients are 0.79 and higher, suggests that the procedures described here produce comparable variables. As a conclusion, we assume that any discrepancy left between both measures is attributable to real variability across and along the shelf. A dynamical analysis of the subtidal SSP field over the northern California shelf and its relationship to other dynamical quantities is reserved for a future paper.

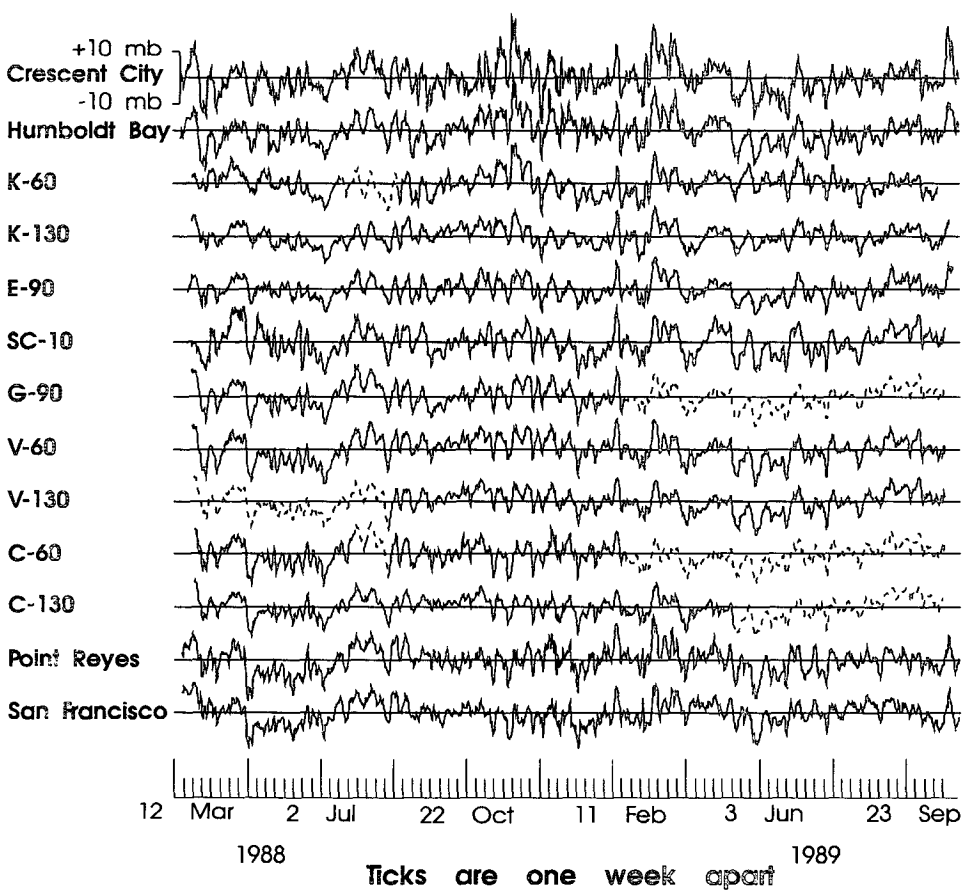

FIG. 10. Low-pass-filtered synthetic subsurface pressure fluctuations in the NCCCS region. Dashed parts of the time series are predicted from neighboring stations using a multiple linear regression model.

TABLE 5. Maximum lagged correlation (upper-left triangle) and lag (lower-right triangle) in hours between SSP fluctuations measured during the NCCCS. Positive lag corresponds to SSP at stations displayed on the vertical axis leads SSP at stations displayed on the horizontal axis. The calculation is done for 6-h samples of SSP. The 95% significance level is 0.4.

	SF	PR	C	V	G	HU	E	K	CR
CR	0.52	0.60	0.63	0.74	0.78	0.87	0.81	0.83	1/0
K	0.46	0.57	0.67	0.75	0.79	0.84	0.87	1/0	−6
E	0.50	0.61	0.79	0.88	0.82	0.87	1/0	0	−6
HU	0.46	0.59	0.65	0.81	0.79	1/0	6	6	0
G	0.67	0.74	0.87	0.91	1/0	0	6	6	0
V	0.67	0.79	0.94	1/0	6	6	12	12	6
C	0.72	0.79	1/0	6	12	12	18	18	12
PR	0.86	1/0	6	12	18	18	18	18	18
SF	1/0	0	6	12	12	18	24	24	24

Acknowledgments. Funding for this study was provided by the Minerals Management Service of the U.S. Department of the Interior under Cooperative Agreement 14-35-0001-30571.

APPENDIX

Temperature Sensitivity of Pressure Sensors

The errors associated with the temperature sensitivity of the Paroscientific pressure sensors depend both on the temperature and the applied pressure. The sensors used during the NCCCS were calibrated prior to and after the experiment over the sensor's full-scale pressure range at several temperatures ranging from 6° to 14°C and a least-squares fit was made to the calibration data taken over all temperatures and pressures. The sensor's temperature was recorded during the deployment of the sensor, and the temperature-dependent pressure calibrations were applied to the sensor's output. Table A1 lists the results of the temperature sensitivity study for each of the sensors used in the NCCCS over the temperature range measured during the sensor's de-

TABLE A1. Temperature sensitivity of pressure sensors deployed during the NCCCS. The sensors are referred to by their serial number (column 1) and their upper operational range (column 2). Column 3 indicates station ID and depth of deployment as well as time of deployment (1—March 1988–August 1988; 2—August 1988–March 1989; 3—March 1989–October 1989). Columns 4–7 give the mean, maximum, and minimum values and standard deviation of temperature at the depth in which the sensors were deployed. Columns 8 and 9 list the temperature sensitivity $\Delta P/\Delta T$ of the individual sensors for the temperature range in which they were deployed. Column 10 lists standard deviations of the pressure differences ΔP between pressures calibrated at a constant temperature of 6°C and pressure calibrated using the temperature dependent calibration equation.

Serial number	Full range (db)	Deployed at	Temperature (°C)				$\Delta P/\Delta T$ (mb °C^{-1})		ΔP std (mb)
			Mean	Std	Max	Min	Max	Min	
1114	31	SC-10/1	10.17	1.31	13.11	7.75	0.80	−0.63	0.50
		SC-10/3	10.74	1.15	12.92	8.12	1.15	−0.43	0.62
9065	31	SC-10/2	10.76	1.17	12.93	8.36	−0.13	−0.75	0.32
8019	138	V-60/1	8.36	0.62	9.85	7.14	1.13	0.50	0.64
		C-60/2	9.95	0.42	11.04	9.04	1.11	0.78	0.33
12 959	138	G-90/1	7.92	0.59	9.07	6.67	0.43	−0.44	0.12
		K-60/2	9.22	0.84	12.25	8.09	0.08	−0.48	0.34
12 960	138	E-90/1	7.79	0.48	8.77	6.88	0.15	−0.09	0.02
30 101	138	K-60/1	8.14	0.56	9.32	6.81	0.30	−0.34	0.13
		E-90/2	8.95	0.51	10.88	8.14	0.21	−0.49	0.22
33 539	138	G-90/2	9.06	0.38	10.16	8.06	−0.04	−0.24	0.05
		E-90/3	8.59	0.63	10.52	7.43	0.02	−0.28	0.07
33 542	138	C-60/1	8.54	0.78	10.46	7.45	1.46	−0.41	0.84
		V-60/3	9.08	0.86	11.02	7.49	1.46	−0.41	1.02
34 070	138	V-60/2	9.70	0.51	11.38	8.60	0.21	−0.17	0.06
		K-60/3	8.39	0.71	10.28	7.24	0.22	0.05	0.14
18 251	276	C-130/1	8.14	0.39	8.95	7.31	0.27	−0.26	0.06
		K-130/2	8.53	0.33	9.49	7.82	0.27	0.04	0.08
18 709	276	K-130/1	7.54	0.46	8.68	6.79	1.45	0.84	0.62
		C-130/3	8.33	0.38	9.18	7.25	1.45	0.58	0.49
32 749	276	C-130/2	8.94	0.30	9.63	7.90	1.06	0.58	0.30
		V-130/3	8.11	0.57	9.38	6.85	1.06	−0.74	0.38
32 750	276	V-130/2	8.58	0.36	9.43	7.59	0.04	−0.10	0.01
		K-130/3	7.98	0.58	9.53	6.68	0.05	−0.11	0.01

ployment. The changes in indicated pressure (ΔP) are calculated relative to the indicated pressure measured at 6°C. Standard deviations of ΔP are listed in column 10 of Table A1. The temperature sensitivities $\Delta P/\Delta T$ (columns 8 and 9, Table A1) are in general smaller than $|\pm 1|$ mb $°C^{-1}$ over the temperature range measured during deployment of the sensors (columns 6 and 7, Table A1). Two exceptions are the 138-db sensor 8019 and the 276-db sensor 18 709, which show sensitivities as large as 1.5 mb $°C^{-1}$. Qualitatively, the results presented in this paper are not affected by the sensor's temperature sensitivity.

REFERENCES

Agnew, D. C., 1986: Detailed analysis of tide gauge data: A case history. *Mar. Geod.*, **10**, 231–255.

Allen, J. S., and R. L. Smith, 1981: On the dynamics of wind-driven shelf currents. *Philos. Trans. Roy. Soc. London*, **A302**, 617–634.

Brown, W. S., J. D. Irish, and A. Bratkovich, 1983: CODE-1: Moored temperature and conductivity observations. CODE-1: Moored Array and Large Scale Data Report. WHOI Tech. Rep. 82-83, CODE Tech. Rep. 21, Woods Hole Oceanogr. Inst., Woods Hole MA, 32 pp.

——, N. R. Pettigrew, and J. D. Irish, 1985: The Nantucket Shoals Flux Experiment (NSFE). Part II: The structure and variability of across-shelf pressure gradients. *J. Phys. Oceanogr.*, **15**, 749–771.

——, J. D. Irish, and C. D. Winant, 1987: A description of subtidal pressure field observations on the northern California continental shelf during the Coastal Ocean Dynamics Experiment. *J. Geophys. Res.*, **92**(C2), 1605–1635.

C&GS, 1965: Manual of Tide Observations. Publication 30-1, Coast and Geodetic Survey, U.S. Department of Commerce, Washington, D.C., 72 pp.

Chapman, D. C., 1987: Application of wind-forced, long, coastal-trapped wave theory along the California coast. *J. Geophys. Res.*, **92**(C2), 1798–1816.

Christensen, N., Jr., R. de la Paz V., and G. Guiterrez V., 1983: A study of sub-inertial waves off the west coast of Mexico. *Deep-Sea Res.*, **30**, 835–850.

Davis, R. E., and P. S. Bogden, 1989: Variability on the California shelf forced by local and remote winds during the Coastal Ocean Dynamics Experiment. *J. Geophys. Res.*, **94**(C4), 4763–4783.

Dobson, F. A., 1980: Air pressure measurement techniques. *Air-Sea Interactions, Instruments and Methods*, F. Dobson, L. Hasse, and R. Davis, Eds., Plenum Press, 231–254.

Enfield, D. B., and J. S. Allen, 1980: On the structure and dynamics of monthly mean sea level anomalies along the Pacific coast of North and South America. *J. Phys. Oceanogr.*, **10**, 557–578.

Erdman, M. R., 1983: Observations of bottom pressure on the continental shelf. Ph.D. dissertation, Scripps Institution of Oceanography, University of California, San Diego, La Jolla, CA, 96 pp.

Hickey, B. M., and N. E. Pola, 1983: The seasonal alongshore pressure gradient on the west coast of the United States. *J. Geophys. Res.*, **88**(C12), 7623–7633.

Huyer, A., 1984: Hydrographic observations along the CODE central line off northern California, 1981. *J. Phys. Oceanogr.*, **14**, 1647–1658.

Largier, J. L., B. A. Magnell, and C. D. Winant, 1993: Subtidal circulation over the northern California shelf. *J. Geophys. Res.*, **98**(C10), 18 147–18 179.

Lennon, G. W., 1967: A critical examination of the conventional tide gauge. *Proc. Symp. on Tides*, Monaco, UNESCO, 29–43.

Lentz, S. J., 1993: The accuracy of tide gauge measurements at subtidal frequencies. *J. Atmos. Oceanic Technol.*, **10**, 238–245.

——, and C. D. Winant, 1986: Subinertial currents on the southern California shelf. *J. Phys. Oceanogr.*, **16**, 1737–1750.

Limeburner, R., 1985: Code 2: Moored array and large-scale data report. CODE Tech. Rep. No. 38, WHOI Tech. Rep. 85–35, 234 pp.

Magnell, B. A., and coauthors, 1989: Northern California Coastal Circulation Study data report No. 2: Main Measurement Program March-August 1988. Tech. Rep., Department of Interior, Minerals Management Service, EG&G WASC Oceanographic Services Rep. No. NCCCS-89-17, Waltham, MA, 442 pp.

Munk, W. H., F. Snodgrass, and M. Wimbusch, 1970: Tides offshore: Transition from California coastal to deep-sea waters. *Geophys. Fluid Dyn.*, **1**, 161–235.

Shih, H. H., and D. L. Porter, 1981: Error models for stilling well-float type tide gauges. Oceans 1981 Conference Report, 2, 1118–1124.

Strub, P. T., J. S. Allen, A. Huyer, R. L. Smith, and R. C. Beardsley, 1987: Seasonal cycles of currents, temperatures, winds, and sea level over the northeast Pacific continental shelf: 35°N to 48°N. *J. Geophys. Res.*, **92**(C2), 1507–1526.

Wearn, R. B., Jr., and N. G. Larson, 1982: Measurements of the sensitivities and drift of Digiquartz pressure sensors. *Deep-Sea Res.*, **29**, 111–134.

Winant, C. D., R. C. Beardsley, and R. E. Davis, 1987: Moored wind, temperature, and current observations made during Coastal Ocean Dynamics Experiments 1 and 2 over the northern California continental shelf and upper slope. *J. Geophys. Res.*, **92**(C2), 1569–1604.